ACS Sustainable Chemistry & Engineering

pubs.acs.org/journal/ascecg

Research Article

Rapid Transformation of Furfural to Biofuel Additive Ethyl Levulinate with In Situ Suppression of Humins Promoted by an Acidic-Oxygen Environment

Surachai Karnjanakom,* Asep Bayu, Panya Maneechakr, Chanatip Samart, Suwadee Kongparakul, and Guoqing Guan

Cite This: https://doi.org/10.1021/acssuschemeng.1c04606

Read Online

ACCESS | Metrics & More | Article Recommendations | Supporting Information

ABSTRACT: Sustainable production of biofuel additive ethyl levulinate (EL) from biomass-derived furfural (FF) is an interesting way owing to its application in improving the diesel combustion process without the expense of octane number. In this study, a stable mesoporous SO_3H@Ni−Al catalyst prepared via facile a hydrothermal-functionalization process was characterized and applied for ultrasound-assisted transformation of FF into EL using ethanol as a hydrogen donor. Interestingly, the formation of humins in the mixture solution and on the catalyst surface was effectively suppressed after introduction of an oxygen environment, resulting from an oxidative degradation reaction. The optimization process was carried out under catalyst acidity, ultrasonic power generation, and statistical design. As desired, a high yield of EL (~97%, E_a = 25.95 kJ/mol) without humins' formation was well achieved in a shorter reaction time (95 min) and at a low reaction temperature (112 °C), compared with a previous conventional reaction. Moreover, the introduction of oxygen strongly promoted the catalyst reusability with a slight reduction in its catalytic behavior, while selectivity/distribution in the liquid product had slight differentiation.

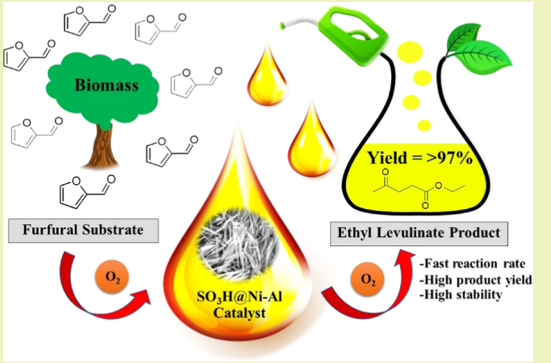

KEYWORDS: *biofuel additive, furfural, ethyl levulinate, humins, SO_3H@Ni−Al catalyst*

INTRODUCTION

Due to the drastic decrease of fossil fuel resources in the past few years, investigating a renewable energy resource has attracted a lot of attention.[1,2] Biomass-derived furfural is a good candidate that can be further upgraded for sustainable production of biofuels and value chemicals such as ethyl levulinate (EL), γ-valerolactone (GVL), 2-(diethoxymethyl)-furan (DTMF), and others.[3−6] As such, some advantages in EL properties are evidently revealed as follows: (I) excellent flashpoint and combustion stabilities are found since it has an energy density of about 24.8 MJ/L, compared to EtOH (~24 MJ/L) and gasoline (~35.2 MJ/L), and (II) it can be utilized as a biofuel additive or blend in diesel engine due to its unique ability to suppress CO, CO_2, and NO_x emissions.[7−9] In a commercial way, as known, EL is produced from levulinic acid (LA), furfural (FF), furfuryl alcohol (FA), 5-hydroxymethyl-furfural (HMF), or carbohydrates via principal reactions such as ethanolysis and etherification over a homogeneous acid catalyst and EtOH as well as a H_2 source.[10] Nevertheless, several advantages of the homogeneous acid catalyst including fast reaction rate, high yield and selectivity of products, and low price have been exposed, but it also has some disadvantages such as corrosive conditions in equipment/environment and difficult/complex recycling.[11,12] Also, the cost in an industrial process may be increased to some extent due to H_2 consumption in large amounts or high operation pressures.

From the above intentions, many researchers have tried to develop several heterogeneous acid catalysts bearing Lewis and Brønsted acid sites for EL production.[13−16] Guo et al.[17] studied the EL production from FAL over an amino-sulfonated functional carbon catalyst, and the results indicated that an EL yield of 65% was obtained at 150 °C for 6 h. Zhu et al.[18] achieved conversion of furfural into EL (EL yield = 77.6%) without an external H_2 source at 120 °C for 24 h over a Au-$HSiW/ZrO_2$ catalyst. Tang et al.[19] found that a maximum EL yield of 55% was obtained from FF conversion catalyzed by Zr-SBA-15 at 180 °C for 18 h via tandem reactions between FF hydrogenation and FAL ethanolysis. They also reported that a

Received: July 7, 2021
Revised: September 27, 2021

combination of Lewis and Brønsted acid sites on the as-prepared catalyst resulted in facile production of EL via the last step of ring opening in ethyl furfuryl ether (EFE). As reported in previous literature studies, a high EL yield of >90% from FF conversion may be achieved since a long reaction time and high reaction temperature as well as an active acid catalyst are required, leading to a very high production cost. Moreover, the main problem during the EL production process is the coformation of humins in the solvent system and on the catalyst surface via polymerization/condensation, resulting in low EL yield and rapid deactivation of catalysts.[20−22]

To solve the above problems, a stable mesoporous SO_3H@Ni−Al catalyst was developed via facile hydrothermal and functionalization processes with the assistance of cationic surfactant cetyltrimethylammonium bromide (CTAB) and chlorosulfonic acid (CA). Here, a mesoporous catalyst was carefully selected since it had high surface area/large pore size (easily accessible active sites), suitable acidity (easily accessible Lewis and Brønsted acid sites), and good thermal stability.[23] The textural, morphological, and chemical properties of the catalyst were systematically characterized in detail. The environmental behaviors for O_2 and N_2 introduction in the system were tested and compared to obstruct the coformation of humins and to enhance the long-term stability of the catalyst during the FF conversion into EL. To increase the reaction rate for selective formation of EL, ultrasonic power generation was applied, compared to the conventional stirring system. Various effects including the catalyst type, catalyst loading amount, ultrasonic power, O_2 and N_2 atmosphere conditions, alcoholic solvent, reaction temperature, and time were studied along with the optimization processes for EL production using an integration of 2^k factorial and Box−Behnken designs as well as kinetic reaction/activation energy. The possible mechanisms for EL formation and humin suppression under the as-developed system were discussed. The efficiency of the as-selected catalyst was compared with the commercial catalyst based on the turnover rate (TOR) for conversion of FF into EL. Moreover, to confirm the long-term stability of the catalyst, the reusability test was performed under an O_2 and N_2 atmosphere. This work not only provides a facile way that enables the production of EL with high yield as well as the retention of catalyst stability but also is highly expected to be further applied in practical processes.

EXPERIMENTAL SECTION

Preparation of Ni−Al Support. Herein, the molar compositions were fixed as follows: 0.9Al:0.1Ni:1.2CTAB:85H_2O:4.6CH_4N_2O for support preparation via hydrothermal and functionalization processes. First, the exact amounts of urea, aluminum nitrate, and nickel nitrate were mixed with distilled water and stirred at ambient temperature for 1 h. The CTAB surfactant was introduced and severely stirred until a homogeneous solution was obtained. Then, the solution was heated at 150 °C for 12 h under hydrothermal conditions. The formed solid product was separated by filtration, washed with distilled water, and dried at 105 °C. Finally, the solid product was heated at 650 °C for 2 h under calcination to obtain the mesoporous Ni−Al catalyst.

Preparation of SO_3H@Ni−Al Catalyst. First, 1.0 g of support and 20 mL of dichloromethane were mixed using setup equipment consisting of a suction + dropping funnel. Then, an exact amount of CA was carefully dropped into the resulting mixture and stirred for 2 h at ambient temperature. During this functionalization process, the produced gas was trapped by the $CaCl_2$ section with a vacuum system, while surplus HCl was separated by the suction process. Finally, the SO_3H@Ni−Al catalyst was washed with ethanol and distilled water and dried at 105 °C. It should be mentioned here that the as-prepared catalysts were denoted SO_3H@Ni−Al-(0), SO_3H@Ni−Al-(1), SO_3H@Ni−Al-(2), SO_3H@Ni−Al-(3), and SO_3H@Ni−Al-(4) based on the weight ratios of CA to Ni−Al of 0/1, 1/1, 2/1, 3/1, and 4/1, respectively. The details of the characterization method of the as-prepared catalyst including N_2 sorption, X-ray diffraction (XRD), scanning electron microscopy−energy dispersive X-ray spectroscopy (SEM−EDS), transmission electron microscopy (TEM), thermogravimetric analysis−derivative thermogravimetry (TGA−DTG), NH_3-temperature-programmed desorption (TPD), and Py-Fourier transform infrared (FTIR) techniques are given in the Supporting Information (SI).

Catalytic Transformation of FF to EL. Herin, the EL production process was carried out in a three-necked, round-bottom flask equipped with a gas tube, an ultrasonic probe, and a reflex condenser. First, an exact amount of catalyst and 1.0 g of FF substrate were added to 20 mL of ethanol. The reaction was conducted using ultrasonic frequency at 2500 Hz with a stirring speed at 650 rpm. During the reaction, O_2 or N_2 gas was introduced inside the reactor at a flow rate of 20 mL/min. Various effects such as the weight ratio of CA to Ni−Al (0−4), ultrasonic power generation (0−100 W), catalyst loading amount (0.1−0.5 g), reaction temperature (70−140 °C), and reaction time (30-120 min) were systematically investigated via cointegration of 2^k factorial and Box−Behnken designs. The details on these experimental designs are provided in the SI.[24] After finishing the process, the reaction was immediately stopped by soaking in a cooling bath. Prior to the reusability study, the spent catalyst was separated by the centrifugation technique along with washing with ethanol + distilled water and drying at 105 °C.

Chemical Product Analysis. Chemical liquid products such as FF substrate, EL, and others were qualitatively analyzed by gas chromatography (Agilent instrument) equipped with a flame ionization detector (GC-FID) including a capillary Agilent HP-5 column (30.0 m × 0.25 mm × 0.25 μm). The temperature programs are as follows: 313 K (4 min) − 5 K/min − 523 K (5 min). N_2 was utilized as a carrier gas at a flow rate of 1.0 mL/min. The concentrations (% mol) in each product were calculated using a dodecane sample as an internal standard.

RESULTS AND DISCUSSION

Textural, Morphological, and Chemical Properties of Catalysts. Figure 1A presents the N_2 sorption isotherms of different catalysts. One can see that the isotherms with type IV were found for all catalysts, according to an ordered mesoporous structure.[25,26] Figure 1B presents the pore size distributions of different catalysts. The narrow distributions with a pore size range of around 2.5−3.5 nm were observed for all catalysts, while the pore volume of the catalyst was reduced to some extent with an increase in the weight ratio of CA to Ni−Al from 0 to 4. This also indicated that the mesoporous structure of the catalyst was still maintained after the functionalization process was applied. Physical properties such as the surface area, pore volume, and pore size are provided in Table 1. As related, the pore size of the SO_3H@Ni−Al catalyst did not significantly change, while its surface area and pore volume were clearly decreased after an increase in the weight ratio of CA to Ni−Al. This might be attributed to well ability for sulfonic distribution on the catalyst structure without pore blockage.

Figure 2 presents the XRD patterns of SO_3H@Ni−Al-(0) and SO_3H@Ni−Al-(3) at small/wide-angle X-ray scattering. As shown in Figure 2A, three diffraction peaks at 2.2, 3.8, and 4.4° should be ascribed to [100], [110], and [200] planes, respectively, suggesting mesoporous material with the hexagonal structure. In Figure 2B, crystalline peaks of the γ-alumina structure appeared at 32.6, 36.6, 39.5, 45.8, 60.6, and 67.2°, corresponding to the reflections on [220], [311], [222],

https://doi.org/10.1021/acssuschemeng.1c04606
ACS Sustainable Chem. Eng. XXXX, XXX, XXX−XXX

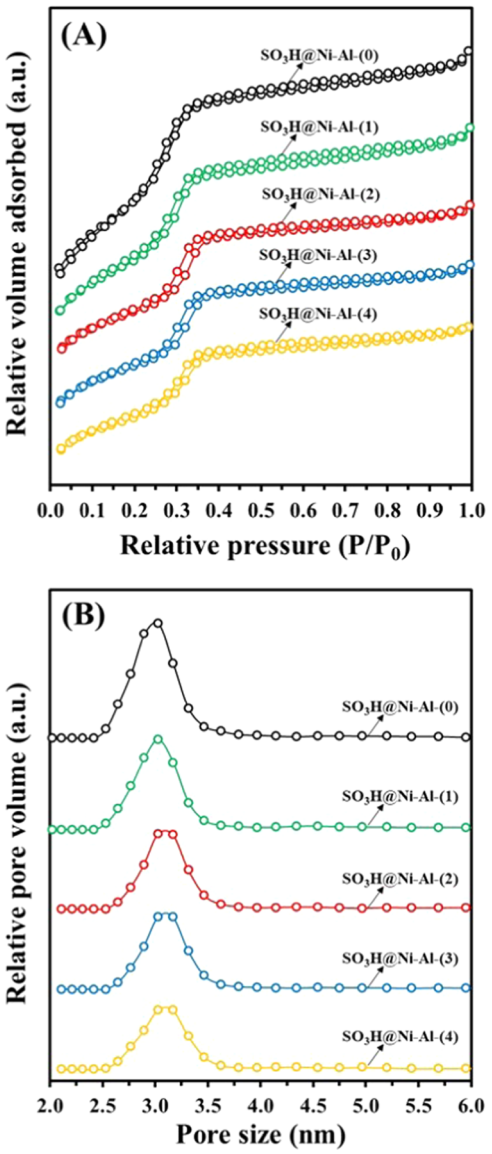

Figure 1. (A) N_2 sorption isotherms and (B) pore size distributions of various acid catalysts.

Table 1. Physicochemical Properties of Various Catalysts

catalyst	surface area (m^2/g)	pore volume (cm^3/g)	pore size (nm)	acidity (mmol/g)
SO_3H@Ni−Al-(0)	748	1.05	3.27	0.64
SO_3H@Ni−Al-(1)	731	0.98	3.25	1.42
SO_3H@Ni−Al-(2)	716	0.92	3.25	2.11
SO_3H@Ni−Al-(3)	702	0.85	3.24	2.53
SO_3H@Ni−Al-(4)	673	0.77	3.21	3.20
SO_3H-Al_2O_3	205	0.86	9.16	1.94
SO_3H-ZSM-5	342	0.38	0.41	1.73
SO_3H-activated carbon	844	1.20	2.27	1.22
SiO_2-tosic acid	279	0.77	9.85	0.80
Amberlyst-35	52	0.62	30.14	5.20
spent SO_3H@Ni−Al-(3)[a]	689	0.84	3.22	2.49
spent SO_3H@Ni−Al-(3)[b]	323	0.19	1.58	2.43

[a]Spent SO_3H@Ni−Al-(3) after the reusability test under an oxygen environment. [b]Spent SO_3H@Ni−Al-(3) after the reusability test under a nitrogen environment.

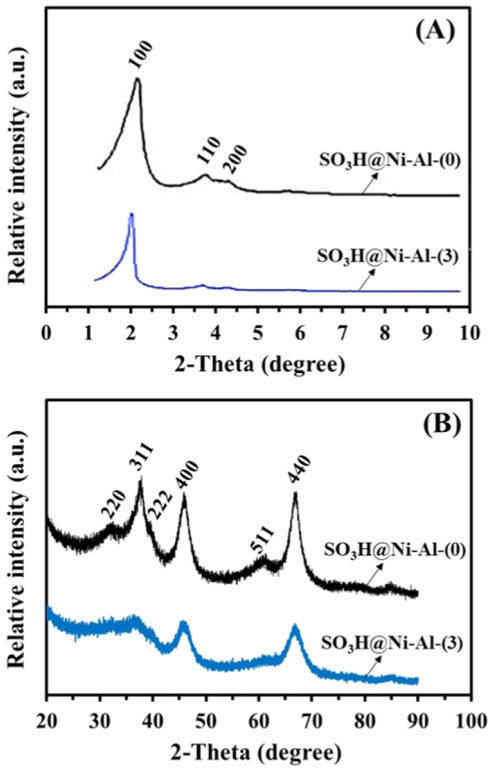

Figure 2. XRD patterns of SO_3H@Ni−Al-(0) and SO_3H@Ni−Al-(3) using (A) small- and (B) wide-angle X-ray scattering.

[400], [511], and [440] planes, respectively. It should be mentioned here that no diffraction peaks of NiO were observed in this study, resulting from its homogeneous dispersion in the SO_3H@Ni−Al structure. For comparison, after the functionalization process such as SO_3H@Ni−Al-(3), the apparent reduction of the XRD peak occurred without any shifting of the pattern, indicating that sulfonic introduction on the Ni−Al support had a nonsignificant influence on destruction of the ordered mesoporous structure.

Figure 3 presents the TEM and SEM−energy dispersive X-ray analysis (EDX) images of SO_3H@Ni−Al-(0) and SO_3H@Ni−Al-(3). In Figure 3A,B, the ordered mesoporous network at the [110] plane was observed for both samples, confirming that a hexagonal mesoporous structure still existed after the functionalization process was applied. In Figure 3C,D, the similar rodlike morphologies were revealed along with the uniform shape/particle for both catalysts, indicating that their morphologies did not destroy after the modification process. Good distribution patterns of Al, Ni, and S elements on SO_3H@Ni−Al-(3) were also supported using EDX mapping images (Figure 3E−G). The formation behavior of the rodlike structure was controlled using urea as a precipitant substrate. Herein, the pH value in the resulting mixture was increased via thermal decomposition of urea to NH_3 and CO_2 gases. In this case, aluminum carbonate hydroxide formed and further interacted with the CTAB surfactant, resulting in reformation of the rodlike structure as-prepared catalyst/support.[27,28] It should be mentioned here that the molar composition of Ni was fixed at 0.1 since it could homogeneously occur with Al. Higher compositions could lead to heterogeneous phases.

Figure 4 presents the chemical properties of SO_3H@Ni−Al catalysts, which were investigated by NH_3-TPD and Py-FTIR analyses. In Figure 4A, for SO_3H@Ni−Al-(0) without a

https://doi.org/10.1021/acssuschemeng.1c04606
ACS Sustainable Chem. Eng. XXXX, XXX, XXX−XXX

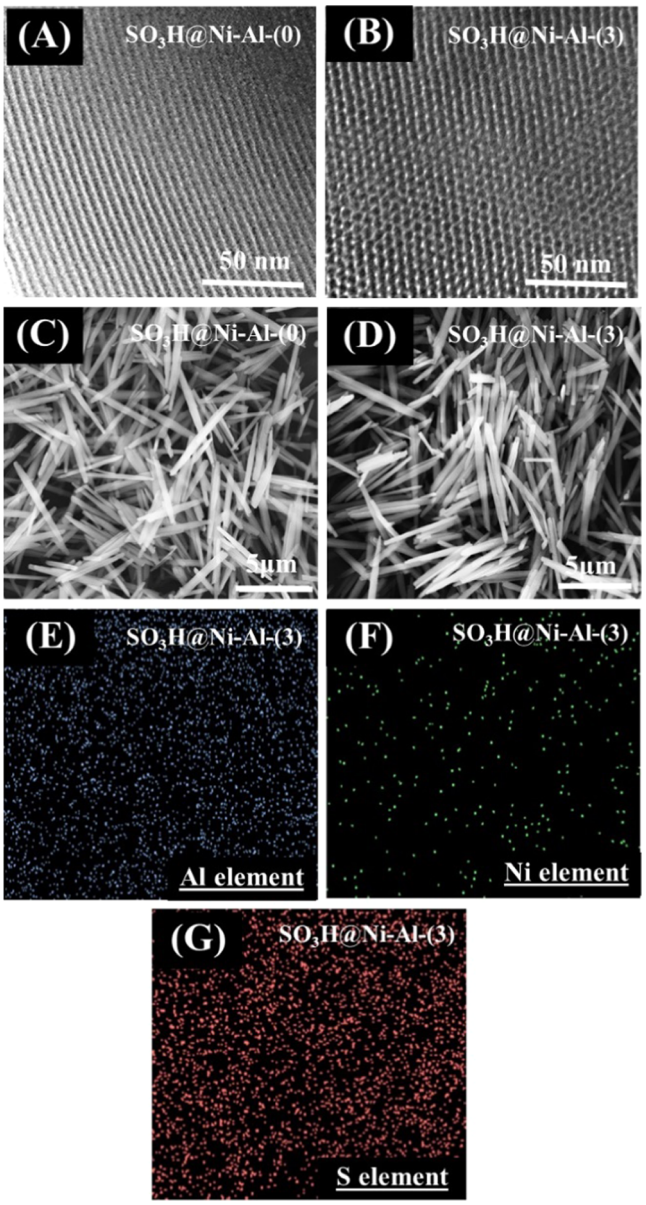

Figure 3. (A), (B) TEM images, (C), (D) SEM images of SO_3H@Ni−Al-(0) and SO_3H@Ni−Al-(3), and (E)−(G) EDX mapping images of SO_3H@Ni−Al-(3).

sulfonic functionalization process, one main peak of NH_3desorption appears at a low temperature of ∼140 °C, which could be ascribed to weak acid sites/Lewis acid sites.[29−31] Interestingly, with an increase of CA amount such as SO_3H@Ni−Al-(1) to SO_3H@Ni−Al-(3), the NH_3 desorption peaks shifted to the higher temperature, while the intensities of peaks at the temperature range of around 150−300 °C increased, resulting from new creation of a strong acid site/Brønsted acid. Remarkably, for SO_3H@Ni−Al-(4), the intensity of NH_3 desorption peaks at the highest temperature was significantly reduced, while the density of medium acid sites was higher than the other ones. This suggests that the presence of an excessive number of sulfonic groups tremendously covered the catalyst surface, while some Lewis acid sites in the alumina structure were destroyed during the functionalization process. On the other hand, the different locations of the sulfonic group on the catalyst structure might

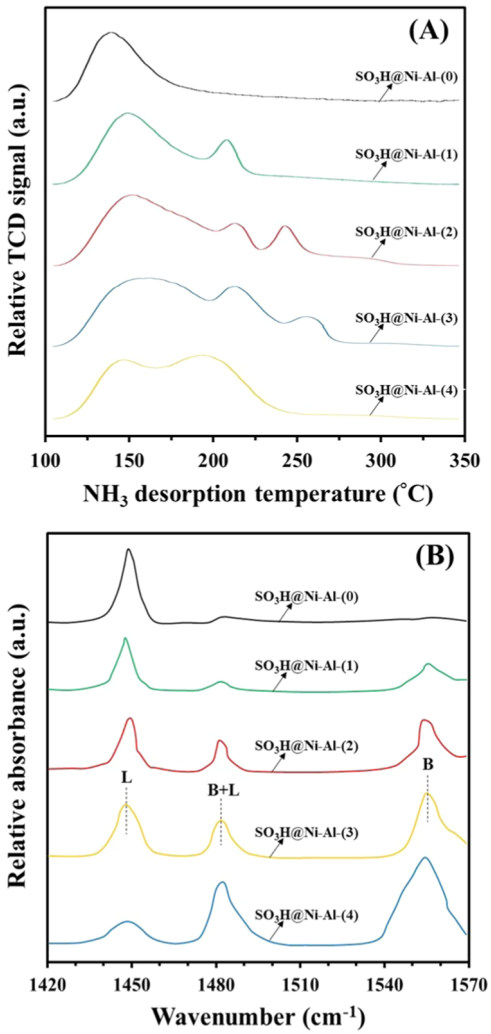

Figure 4. (A) NH_3-TPD profiles and (B) Py-FTIR spectra of various acid catalysts.

Table 2. Lewis and Brønsted Acid Amounts on Various Acid Catalysts

catalyst	Lewis acid amount (mmol/g)	Brønsted acid amount (mmol/g)	L/B ratio
SO_3H@Ni−Al-(0)	0.64	0.00	
SO_3H@Ni−Al-(1)	0.62	0.80	0.78
SO_3H@Ni−Al-(2)	0.61	1.50	0.41
SO_3H@Ni−Al-(3)	0.62	1.91	0.32
SO_3H@Ni−Al-(4)	0.47	2.73	0.17
SO_3H-Al_2O_3	0.37	1.57	0.24
SO_3H-ZSM-5	0.21	1.52	0.14
SO_3H-activated carbon	0.03	1.19	0.03
SiO_2-tosic acid	0.69	0.11	6.27
Amberlyst-35	0.00	5.20	

be a part of acid dispersion behavior. The acidity and L/B ratio of each catalyst are shown in Tables 1 and 2, respectively. As expected, the increase of the CA to Ni−Al ratio from 1 to 4 resulted in an increase of acidity from 1.42 to 3.20 mmol/g, while the L/B ratios decreased from 0.78 to 0.17.

In Figure 4B, Py-FTIR spectra at 200 °C were applied to confirm the existence of Lewis and Brønsted acidic sites on the SO_3H@Ni−Al catalyst. Here, the predominant bands appear-

https://doi.org/10.1021/acssuschemeng.1c04606
ACS Sustainable Chem. Eng. XXXX, XXX, XXX−XXX

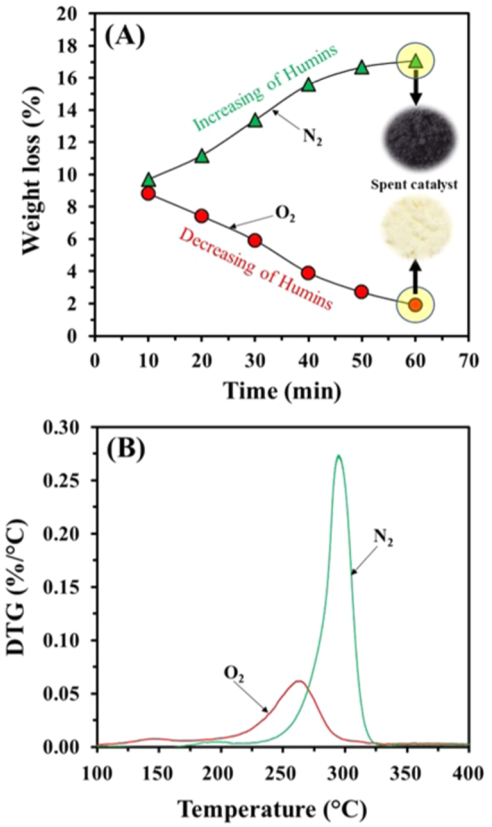

Figure 5. (A) Effect of reaction time on humins' deposition on the spent SO_3H@Ni−Al-(3) catalysts and (B) DTG profiles of spent SO_3H@Ni−Al-(3) catalysts after reaction for 30 min for transformation of FF to EL under the oxygen and nitrogen environments.

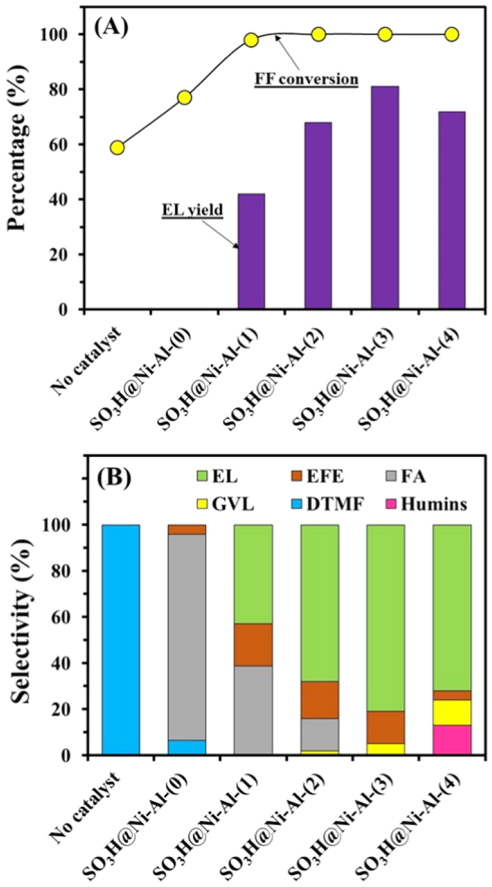

Figure 6. (A) FF conversion with EL yield and (B) chemical distribution in the liquid product in a reaction catalyzed by the oxygen environment based on the effect of catalyst type. Reaction conditions: catalyst amount = 0.5 g, reaction temperature = 140 °C, reaction time = 120 min, ultrasonic power = 80 W.

ing at wavenumbers of 1545, 1490, and 1450 cm^{-1} could be assigned to vibration characteristic of pyridine adsorption on Brønsted acid sites, Brønsted−Lewis acid sites, and Lewis acid sites, respectively.[32] The increase of the sulfonic group amount resulted in an increase of the Brønsted acid site, which was beneficial for the catalytic conversion of FF into EL. This Py-FTIR result was in good agreement with NH_3-TPD analysis. Figure S1 presents the TG-DTG profile of the SO_3H@Ni−Al-(3) catalyst at temperatures of 100−600 °C under oxygen flow. Two mass losses at the ranges around 100−200 and 250−450 °C could be revealed on certain decomposition processes of water and sulfonic groups. Based on this study, it is demonstrated that the SO_3H@Ni−Al catalyst had stability at high temperatures, which could be satisfactorily applied in EL production at the as-selected temperature range.

EL Production from FF Substrate. The role of humins deposited on the spent SO_3H@Ni−Al-(3) catalysts in EL production from FF transformation at a reaction time of 10−60 min under O_2 and N_2 conditions is presented in Figure 5A. Remarkably, the yield of humins' formation on the catalyst continuously reduced with an increase of reaction time when the oxygen environment was applied, indicating that oxidative degradation was well promoted.[33] Meanwhile, the opposite trend was found, and the colors of the catalyst and chemical liquid became dark-brown under oxygen conditions. From this result, it is demonstrated that the oxygen environment under this EL production system promoted the catalyst stability via a humin suppression process. To check the stability in EL production, the catalytic performance was tested as follows: for the first run, the nitrogen environment was introduced under FF transformation for 60 min. Thereafter, for the second run, it was further tested under the oxygen environment without the presence of the FF substrate and nitrogen gas. As predicted, pristine color in the catalyst was obtained from humins' decomposition, indicating that the existence of the oxygen environment was very important for the reaction system. Figure 5B presents the decomposition behavior of humins on the SO_3H@Ni−Al-(3) catalyst after finishing the reaction process via the DTG profile at 100−400 °C. One can see that different thermal decomposition ranges were found, resulting from the presence of humins with different species on the catalyst structure. In the case of the spent catalyst derived from the oxygen environment, the humins on the catalyst were more easily decomposed at a lower temperature of around 265 °C, while higher thermal decomposition of humins (300 °C) was required for the spent catalyst derived from the nitrogen environment. This also suggests that small and big species of humins were preferred to form under oxygen and nitrogen conditions, respectively. Based on the above results, *in situ* suppression of humins could be easily performed in the presence of molecular oxygen, which was highly useful for further regeneration of the spent catalyst at lower temperatures, leading to saving energy consumption.

Figure 6A,B presents the effect of catalyst type on catalytic transformation of FF to EL under the oxygen environment. In

https://doi.org/10.1021/acssuschemeng.1c04606
ACS Sustainable Chem. Eng. XXXX, XXX, XXX−XXX

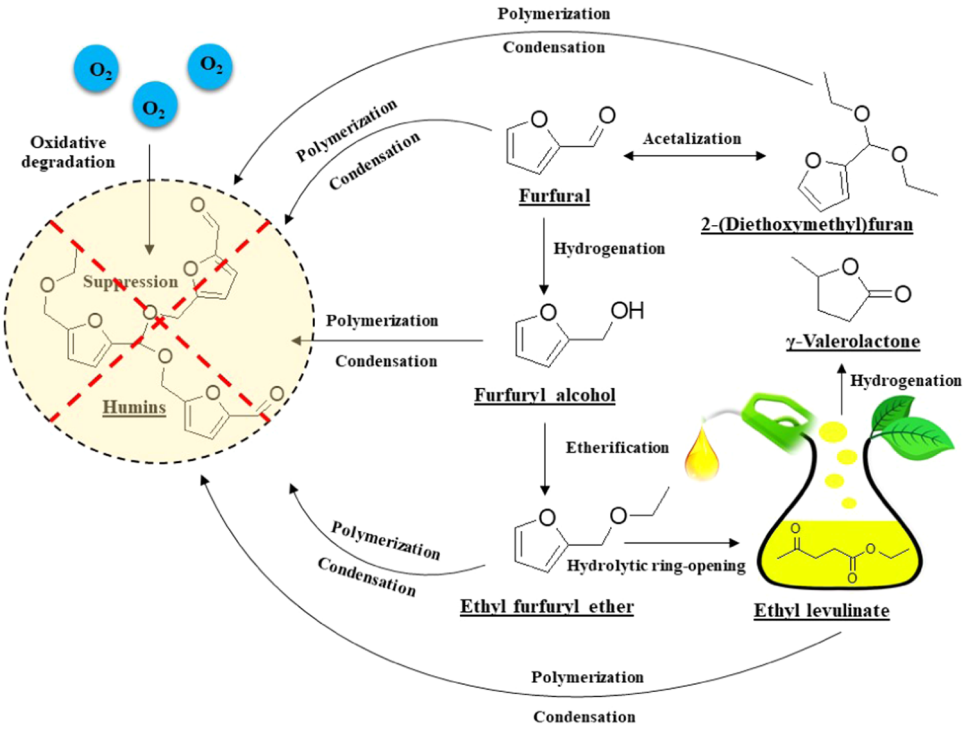

Figure 7. Possible reaction pathways for conversion of FF + EtOH into EL and other chemicals.

this study, the product selectivity was divided into six chemicals such as EL, EFE, FA, GVL, DTMF, and humins. As can be seen, no EL yield was observed in the case of without catalyst loading where even the FF conversion was 59.1%, suggesting that some FF and EtOH were easily acetalized into DTMF via ultrasonic assistance. When SO_3H@Ni−Al-(0) was applied, FF still could not be converted into EL, but the DTMF selectivity significantly decreased with an increase of FA selectivity. This suggests that the acetalization of FF was suppressed via co-contribution of nickel oxide and aluminum oxide catalysts, as well as their Lewis acid sites, and promoted to transfer hydrogenation reactions based on the tandem reaction pathways in Figure 7.[34] This also indicates that reversible acetalization was supported via ultrasonic generation without the assistance of Lewis acid sites from SO_3H@Ni−Al-(0). It should be noted that *in situ* generation of hydrogen without any external addition occurred from an ethanol/hydrogen donor.[35] Also, ethanol was used in an excessive amount of 20 mL to shift the equilibrium forward EL, corresponding to Le Chatelier's principle. Remarkably, the existence of Brønsted acid sites with an increase of CA to Ni−Al ratios from 1 (SO_3H@Ni−Al-(1)) to 3 (SO_3H@Ni−Al-(3)) resulted in the facile formation of EL with an increase of the EL yield from 42.2 to 81.3% and then decrease to some extent using a SO_3H@Ni−Al-(4) catalyst. These behaviors should be described to further generation of GVL and humins' products via second transfer hydrogenation and polymerization/condensation reactions, respectively, when excessive acidity with a L/B ratio of 0.17 existed in the SO_3H@Ni−Al-(4) catalyst. Here, the reaction mechanisms could be explained as follows: (I) FF was converted to FA via transfer hydrogenation with the assistance of Lewis acid Ni−Al catalyst, (II) FA etherification was catalyzed by Lewis/Brønsted acid sites from SO_3H@Ni−Al to form EFE chemical, and (III) EFE was further converted to desired EL via a hydrolytic ring-opening process with the assistance of Brønsted acid sites on the catalyst.[36,37] This indicates that the synergistic effect of Brønsted and Lewis acid sites on SO_3H@Ni−Al catalysts was very important for catalytic production of EL. Based on these results, the SO_3H@Ni−Al-(3) catalyst was chosen to be utilized in the next sections.

Figure 8 presents the effect of ultrasonic application for transformation of FF to EL under the oxygen environment catalyzed by SO_3H@Ni−Al-(3). One can see that a low EL yield of 14.9% was found with the abundant presence of undesired chemicals in the liquid product such as FA, EFE, DTMF, and humins since the ultrasonic generation did not apply. However, when ultrasonic power was generated from 50 to 80 W, the EL yield was significantly increased from 39.3 to 81.3%, indicating that transformation of FF to EL was highly favored with ultrasonic power at 80 W. This should be attributed to the *in situ* production of cavitation bubbles as well as oxidizing species such as hydroxyl and hydrogen radicals from ultrasonic generation, which could strongly catalyze the reaction series, leading to facile formation of EL. Unlikely, the EL yield was reduced to some extent with the increase of ultrasonic power from 80 to 100 W, suggesting that second transfer hydrogenation was replaced by further conversion of EL to GVL, leading to the increase in GVLselectivity in the liquid product.[38] Therefore, an ultrasonic power of 80 W was fixed as the best condition in this study.

To obtain more information on the catalytic system, the integrations of 2^k factorial and Box−Behnken designs as well as kinetic reactions was fully investigated in detail, and the results are provided in the SI (Figures S2−S7 and Tables S1−S3).[39−42] Based on these designs, the highest yield of EL (97.2%) was perfectly produced under the following optimal conditions: catalyst amount = 0.36 g, reaction temperature = 112 °C, reaction time = 95 min, ultrasonic power = 80 W and ultrasonic duty cycle = 60%. The activation energy and pre-

https://doi.org/10.1021/acssuschemeng.1c04606
ACS Sustainable Chem. Eng. XXXX, XXX, XXX−XXX

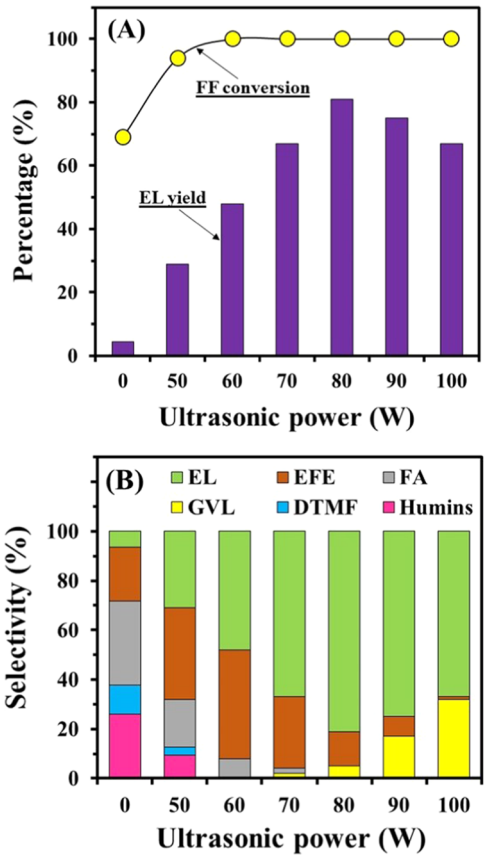

Figure 8. (A) FF conversion with EL yield and (B) chemical distribution in the liquid product under the reaction catalyzed by SO_3H@Ni−Al-(3) and the oxygen environment based on the effect of ultrasonic application. Reaction conditions: catalyst amount = 0.5 g, reaction temperature = 140 °C, reaction time = 120 min, and ultrasonic power = 0−100 W.

exponential values for EL production obtained from the ultrasonic system (25.95 kJ/mol and 1.57×10^2 min^{-1}) were lower when compared with those from the conventional autoclave system (33.37 kJ/mol and 2.85×10^2 min^{-1}). To update our obtained results, the comparison of each catalytic system for EL production from the FF substrate is shown in Table 3.[18−21] The SO_3H@Ni−Al catalyst exhibited better activity than previous catalysts, resulting from proper chemical and physical properties to FF transformation under the as-developed system (entries 1−4 vs 7). Also, higher energy consumption based on higher reaction temperatures and longer reaction times was revealed under the application of autoclave and conventional reflux processes when compared

Table 4. Formation Behaviors of AL and GVL in the Liquid Product Based on Effect of Alcohol Type under the Reaction Catalyzed by SO_3H@Ni−Al-(3) and the Oxygen Environment

entry	alcohol type	conversion (%)	AL yield (%)	GVL yield (%)
1	MeOH	100	98.6	0.0
2	EtOH	100	97.2	0.7
3	*n*-PrOH	100	85.3	6.8
4	*i*-PrOH	100	54.1	32.9
5	*n*-BuOH	100	72.7	15.5
6	*i*-BuOH	100	39.9	48.2

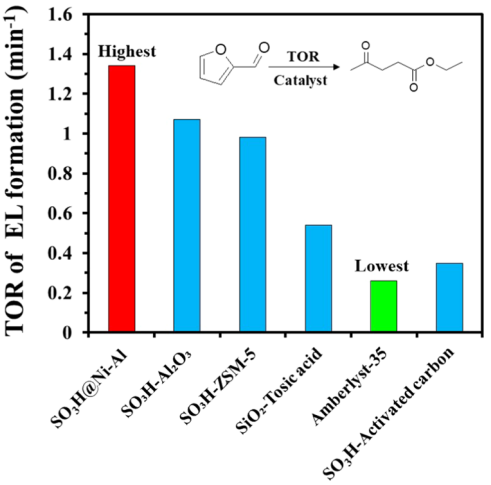

Figure 9. Turnover rate for transformation of FF to EL under the oxygen environment using different catalysts.

with the ultrasonic technique (entries 1−4, 6−9 vs 5). In addition, ultrasonic application not only promotes the reaction kinetic rate but also suppresses the polymerization reaction for humins. Here, the changing in physical properties of liquid chemical and catalyst colors could be observed.

Table 4 presents the effect of alcohol type on transformation of FF to alkyl levulinates (AL) under the oxygen environment catalyzed by SO_3H@Ni−Al-(3). As obtained, the increase of C number in alcohols resulted in a significant reduction of the AL yield in the liquid product, while the GVL yield was increased to some extent. The selectivity for AL production was in the sequence MeOH > EtOH > *n*-PrOH > *n*-BuOH > *i*-PrOH > *i*-BuOH. This indicates that AL was preferred to form in primary alcohols, especially in methanol. However, considering sustainable chemistry, ethanol was still chosen since it was a more eco-friendly chemical. Meanwhile, the opposite trend was found in GVL formation, which was favored in secondary

Table 3. Catalytic Production of EL from FF Substrate by Comparison with Previous Works

entry	catalyst	temperature (°C)	time	catalytic system	EL yield (%)	ref
1	Au-HSiW/ZrO_2	120	24 h	autoclave system + N_2 pressure	77.6	18
2	Zr-SBA-15	180	18 h	autoclave system + N_2 pressure	55.0	19
3	Zr-Al/SBA-15	180	3 h	autoclave system + N_2 pressure	71.4	21
4	Pt/$ZrNbPO_4$	130	6 h	autoclave system + H_2 pressure	75.7	22
5	SO_3H@Ni−Al	112	95 min	ultrasonic system + O_2 atmosphere	97.2	this work
6	SO_3H@Ni−Al	112	95 min	autoclave system + O_2 pressure	64.8	this work
7	SO_3H@Ni−Al	120	6 h	autoclave system + O_2 pressure	87.3	this work
8	SO_3H@Ni−Al	112	95 min	reflux system + O_2 atmosphere	32.5	this work
9	SO_3H@Ni−Al	120	24 h	reflux system + O_2 atmosphere	82.8	this work

https://doi.org/10.1021/acssuschemeng.1c04606
ACS Sustainable Chem. Eng. XXXX, XXX, XXX−XXX

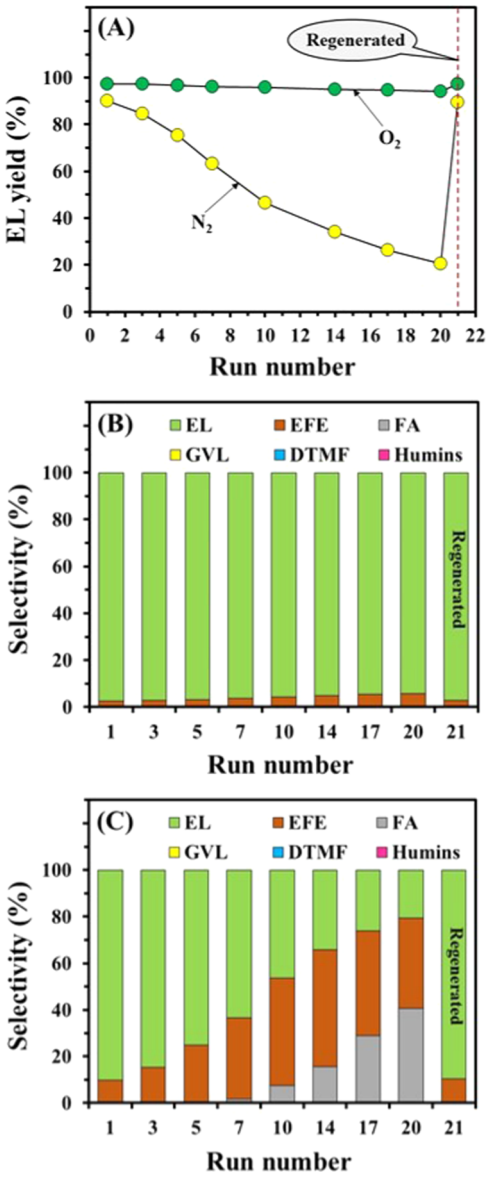

Figure 10. (A) EL yield derived from the reusability effect of SO_3H@Ni−Al-(3) under the oxygen and nitrogen environments. Production distribution derived from the reusability effect of SO_3H@Ni−Al-(3) under environments of (B) oxygen and (C) nitrogen. Reaction conditions: catalyst amount = 0.36 g, reaction temperature = 112 °C, reaction time = 95 min, and ultrasonic power = 80 W.

alcohols, especially for *i*-BuOH, confirming that second transfer hydrogenation was preferred for alcohol with lower reduction potential based on the data of standard molar enthalpy reported in the previous literature.[43]

Catalytic Comparison and Catalyst Reusability. Before study on catalyst reusability, the performance of the as-prepared S-A catalyst was compared with that of various commercial catalysts such as Al_2O_3, ZSM-5, SiO_2-tosic acid, Amberlyst-35, and activated carbon. It should be mentioned here that Al_2O_3, ZSM-5, and activated carbon were functionalized with sulfonic groups using the same method of the S-A catalyst. Figure 9 presents the turnover rate (TOR, min^{-1}) of FF into EL over different catalysts. The value of TOR was calculated by dividing the mole amount of FF that is converted into EL per the catalyst amount with reaction time (mol/g·min) by acidity of the catalyst (mol/g). Here, FF conversion into EL was fixed at 50% for all catalysts to avoid some problems on concentrations of the substate and catalyst. As it can be seen that Amberlyst-35 exhibited poor catalytic activity with the lowest value of TOR, suggesting that FF was converted into humins. As it is known, its excessive acidity with only the existence of the Brønsted acid site of Amberlyst-35 and SO_3H-activated carbon favored promoting the side reactions such as condensation/polymerization. In the cases of SiO_2-tosic acid, poor catalytic performance was observed, resulting from the existence of low acidity with a ratio of L/B = 6.27 (Table 2). Moreover, hard accessibility of reactants into active sites of the catalyst with a low TOR value was found in ZSM-5 (narrow pore size = 0.28 nm) and SO_3H-Al_2O_3 (larger pore size = 9.03 nm) (Table 1). Thus, the S-A catalyst had the best activity for EL production based on the highest value of TOR. Based on these results, S-A had the possibility to be utilized as a promising catalyst for sustainable upgrading of FF into EL in the practical process.

Figure 10 presents the reusability result of SO_3H@Ni−Al-(3) under the oxygen and nitrogen environments. Remarkably, under the oxygen environment, much higher stability of SO_3H@Ni−Al-(3) was found for 20 run number with a slight decrease of the EL yield/selectivity. It demonstrates that oxidative degradation to protect the humins' formation on the catalyst was well promoted by introduction of oxygen without requirement in catalyst regeneration. Unlikely, the catalytic activity based on EL yield under introduction of nitrogen was highly reduced to some extent with an increase of recycling number from the first to the twentieth without any regeneration. Meanwhile, FA and EFE chemicals in liquid products were increased with the incessant reduction of EL selectivity. This should have resulted from catalyst deactivation during the reaction cycle that occurred from humins' formation on the catalyst surface, leading to facile blockage of the porous structure.[44] To ensure this physical deactivation of SO_3H@Ni−Al-(3) without the sulfonic leaching process, the spent catalysts after the 20th run were characterized by Brunauer−Emmett−Teller (BET) and NH_3-TPD. As shown in Table 1, the strong reductions in textural properties such as the surface area and porosity for spent catalysts derived from the reaction cycle under the nitrogen environment were found, while its acidity result did not notably change. Moreover, the spent catalyst after the 20th cycle was further regenerated to remove the humins by only heating at a temperature of 350 °C. As expected, its structure, morphology, and acidic behavior were quite similar to those of the fresh catalyst (Figures S8−S10). In addition, as also shown in Figure 10, the catalytic activity at the 21st cycle was well restored based on EL yield/selectivity, confirming that only the physical deactivation process occurred.

CONCLUSIONS

In summary, SO_3H@Ni−Al was successfully synthesized and applied as a catalyst for ultrasound-assisted transformation of FF into EL under the oxygen environment using ethanol as a hydrogen donor. SO_3H@Ni−Al-(3) with its physiochemical properties such as the high surface area of 702 m^2/g, high thermal stability of >350 °C, and acidity of 2.53 mmol/h (L/B ratio = 0.32) was found to be the best catalyst for EL production. The proper application of the ultrasonic power value for EL production was at 80 W. The introduction of oxygen along with an increase of reaction time was highly beneficial for humins' elimination via an oxidative degradation

https://doi.org/10.1021/acssuschemeng.1c04606
ACS Sustainable Chem. Eng. XXXX, XXX, XXX−XXX

reaction. The use of the SO_3H@Ni−Al catalyst with a lower L/B ratio of 0.32 promoted an undesired polymerization reaction. The GVL chemical could be easily formed via second transfer hydrogenation of EL when too high ultrasonic power and secondary alcohols were applied. The optimal conditions including a catalyst amount of 0.36 g, a reaction temperature of 112 °C, a reaction time of 95 min, an ultrasonic power of 80 W, and an ultrasonic duty cycle of 60% were carried out, providing a maximum EL yield of 97.2% with an activation energy of 25.95 kJ/mol. The physical deactivation of the catalyst could be suppressed by oxygen introduction, leading to excellent reusability. This research is expected for sustainable production of EL with a novel strategy.

■ ASSOCIATED CONTENT

Supporting Information

The Supporting Information is available free of charge at https://pubs.acs.org/doi/10.1021/acssuschemeng.1c04606.

Details of catalyst characterization methods and results and discussion of 2^k factorial and Box−Behnken designs for EL production with an optimum condition (PDF)

■ AUTHOR INFORMATION

Corresponding Author

Surachai Karnjanakom − *Department of Chemistry, Faculty of Science, Rangsit University, Pathumthani 12000, Thailand;* orcid.org/0000-0001-5130-765X; Email: surachai.ka@rsu.ac.th, surachaikarn@gmail.com

Authors

Asep Bayu − *Research Center for Biotechnology, Indonesian Institute of Sciences (LIPI), Bogor 16911 West Java, Indonesia*

Panya Maneechakr − *Department of Chemistry, Faculty of Science, Rangsit University, Pathumthani 12000, Thailand*

Chanatip Samart − *Department of Chemistry, Faculty of Science and Technology, Thammasat University, Pathumthani 12120, Thailand*

Suwadee Kongparakul − *Department of Chemistry, Faculty of Science and Technology, Thammasat University, Pathumthani 12120, Thailand*

Guoqing Guan − *Energy Conversion Engineering Laboratory, Institute of Regional Innovation (IRI), Hirosaki University, Aomori 030-0813, Japan*

Complete contact information is available at: https://pubs.acs.org/10.1021/acssuschemeng.1c04606

Notes

The authors declare no competing financial interest.

■ ACKNOWLEDGMENTS

The authors appreciate the Department of Chemistry, Faculty of Science, Rangsit University, Thailand for supporting all chemicals, equipment, and instruments.

■ REFERENCES

(1) Jiang, S. F.; Sheng, G. P.; Jiang, H. Advances in the Characterization Methods of Biomass Pyrolysis Products. *ACS Sustainable Chem. Eng.* **2019**, *7*, 12639−12655.

(2) Wang, Y.; Meng, X.; Jeong, K.; Li, S.; Leem, G.; Kim, K. H.; Pu, Y.; Ragauskas, A. J.; Yoo, C. G. Investigation of a Lignin-Based Deep Eutectic Solvent Using p-Hydroxybenzoic Acid for Efficient Woody Biomass Conversion. *ACS Sustainable Chem. Eng.* **2020**, *8*, 12542−12553.

(3) Sert, M. Catalytic effect of acidic deep eutectic solvents for the conversion of levulinic acid to ethyl levulinate. *Renewable Energy* **2020**, *153*, 1155−1162.

(4) Dutta, S.; Yu, I. K. M.; Tsang, D. C. W.; Ng, Y. H.; Ok, Y. S.; Sherwood, J.; Clark, J. H. Green synthesis of gamma-valerolactone (GVL) through hydrogenation of biomass derived levulinic acid using non-noble metal catalysts: A critical review. *Chem. Eng. J.* **2019**, *372*, 992−1006.

(5) Dhanalaxmi, K.; Singuru, R.; Mondal, S.; Bai, L.; Reddy, B. M.; Bhaumik, A.; Mondal, J. Magnetic Nanohybrid Decorated Porous Organic Polymer: Synergistic Catalyst for High Performance Levulinic Acid Hydrogenation. *ACS Sustainable Chem. Eng.* **2017**, *5*, 1033−1045.

(6) Soszka, E.; Reijneveld, H. M.; Jędrzejczyk, M.; Rzeźnicka, I.; Grams, J.; Ruppert, A. M. Chlorine Influence on Palladium Doped Nickel Catalysts in Levulinic Acid Hydrogenation with Formic Acid as Hydrogen Source. *ACS Sustainable Chem. Eng.* **2018**, *6*, 14607−14613.

(7) Halder, M.; Bhanja, P.; Islam, M. M.; Chatterjee, S.; Khan, A.; Bhaumik, A.; Islam, S. M. Porous organic polymer as an efficient organocatalyst for the synthesis of biofuel ethyl levulinate. *Mol. Catal.* **2020**, *494*, No. 111119.

(8) Unlu, D.; Ilgen, O.; Hilmioglu, N. D. Biodiesel additive ethyl levulinate synthesis by catalytic membrane: SO42-/ZrO2 loaded hydroxyethyl cellulose. *Chem. Eng. J.* **2016**, *302*, 260−268.

(9) Tiong, Y. W.; Yap, C. L.; Gan, S.; Yap, W. S. P. Kinetic and thermodynamic studies of oil palm mesocarp fiber cellulose conversion to levulinic acid and upgrading to ethyl levulinate via indium trichloride-ionic liquids. *Renewable Energy* **2020**, *146*, 932−943.

(10) Manny, A. J.; Kjelleberg, S.; Kumar, N.; Nys, R. D.; Read, R. W.; Steinberg, P. Reinvestigation of the sulfuric acid-catalysed cyclisation of brominated 2-alkyllevulinic acids to 3-alkyl-5-methyl-ene-2(5H)-furanones. *Tetrahedron* **1997**, *53*, 15813−15826.

(11) Bayu, A.; Abudula, A.; Guan, G. Reaction pathways and selectivity in chemo-catalytic conversion of biomass-derived carbohydrates to high-value chemicals: A review. *Fuel Process. Technol.* **2019**, *196*, No. 106162.

(12) Chithra, P. A.; Darbha, S. Catalytic conversion of HMF into ethyl levulinate − A biofuel over hierarchical zeolites. *Catal. Commun.* **2020**, *140*, No. 105998.

(13) Li, N.; Jiang, S.; Liu, Z. Y.; Guan, X. X.; Zheng, X. C. Preparation and catalytic performance of loofah sponge-derived carbon sulfonic acid for the conversion of levulinic acid to ethyl levulinate. *Catal. Commun.* **2019**, *121*, 11−14.

(14) Zhang, Z.; Yuan, H.; Wang, Y.; Ke, Y. Preparation and characterisation of ordered mesoporous SO42-/Al2O3 and its catalytic activity in the conversion of furfuryl alcohol to ethyl levulinate. *J. Solid State Chem.* **2019**, *280*, No. 120991.

(15) Heda, J.; Niphadkar, P.; Mudliar, S.; Bokade, V. Highly efficient micro-meso acidic H USY catalyst for one step conversion of wheat straw to ethyl levulinate (biofuel additive). *Microporous Mesoporous Mater.* **2020**, *306*, No. 110474.

(16) Russo, V.; Rossano, C.; Salucci, E.; Tesser, R.; Salmi, T.; Serio, M. D. Intraparticle diffusion model to determine the intrinsic kinetics of ethyl levulinate synthesis promoted by Amberlyst-15. *Chem. Eng. Sci.* **2020**, *228*, No. 115974.

(17) Guo, H.; Hirosaki, Y.; Qi, X.; Smith, R. L., Jr. Synthesis of ethyl levulinate over amino sulfonated functional carbon materials. *Renewable Energy* **2020**, *157*, 951−958.

(18) Zhu, S.; Cen, Y.; Guo, J.; Chai, J.; Wanga, J.; Fan, W. One-pot conversion of furfural to alkyl levulinate over bifunctional Au-H4SiW12O40/ZrO2 without external H2. *Green Chem.* **2016**, *18*, 5667−5675.

(19) Tang, K.; Xie, S.; Cofield, G. R.; Yang, X.; Tian, E.; Lin, H. Catalytic transfer hydrogenation of furfural for the production of ethyl

levulinate: Interplay of Lewis and Brønsted acidities. *Energy Technol.* **2018**, *6*, 1826−1831.
(20) Quereshi, S.; Ahmad, E.; Pant, K. K.; Dutta, S. Insights into Microwave-Assisted Synthesis of 5-Ethoxymethylfurfural and Ethyl Levulinate Using Tungsten Disulfide as Catalyst. *ACS Sustainable Chem. Eng.* **2020**, *8*, 1721−1729.
(21) Li, M.; Wei, J.; Yan, G.; Liu, H.; Tang, X.; Sun, Y.; Zeng, X.; Lei, T.; Lin, L. Cascade conversion of furfural to fuel bioadditive ethyl levulinate over bifunctional zirconium based catalysts. *Renewable Energy* **2020**, *147*, 916−923.
(22) Chen, B.; Li, F.; Huang, Z.; Lu, T.; Yuan, Y.; Yuan, G. Integrated Catalytic Process to Directly Convert Furfural to Levulinate Ester with High Selectivity. *ChemSusChem* **2014**, *7*, 202−209.
(23) Maneechakr, P.; Karnjanakom, S. Improving the Bio-Oil Quality via Effective Pyrolysis/Deoxygenation of Palm Kernel Cake over a Metal (Cu, Ni, or Fe)-Doped Carbon Catalyst. *ACS Omega* **2021**, *6*, 20006−20014.
(24) Maneechakr, P.; Karnjanakom, S. A combination of 2k factorial with Box-Behnken designs for FAME production via methanolysis of waste cooking palm oil over low-cost catalyst. *J. Environ. Chem. Eng.* **2019**, *7*, No. 103389.
(25) Malibo, P. M.; Makgwane, P. R.; Baker, P. G. L. Hetero-mixed TiO2-SnO2 interfaced nano-oxide catalyst with enhanced activity for selective oxidation of furfural to maleic acid. *Inorg. Chem. Commun.* **2021**, *129*, No. 108637.
(26) Karnjanakom, S.; Maneechakr, P.; Samart, C.; Guan, G. A facile way for sugar transformation catalyzed by carbon-based Lewis-Brønsted solid acid. *Mol. Catal.* **2019**, *479*, No. 110632.
(27) Dabbagh, H. A.; Shahraki, M. Mesoporous nano rod-like γ-alumina synthesis using phenol−formaldehyde resin as a template. *Microporous Mesoporous Mater.* **2013**, *175*, 8−15.
(28) Contreras, J. L.; Gómez, G.; Zeifert, B.; Salmones, J.; Vázquez, T.; Fuentes, G. A.; Navarrete, J.; Nuño, L. Synthesis of Pt/Al2O3 catalyst using mesoporous alumina prepared with a cationic surfactant. *Catal. Today* **2015**, *250*, 72−86.
(29) Karnjanakom, S.; Bayu, A.; Xiaoketi, P.; Hao, X.; Kongparakul, S.; Samart, C.; Abudula, A.; Guan, G. Selective production of aromatic hydrocarbons from catalytic pyrolysis of biomass over Cu or Fe loaded mesoporous rod-like alumina. *RSC Adv.* **2016**, *6*, 50618−50629.
(30) Yu, Z.; Tian, H.; Sun, K.; Shao, Y.; Zhang, L.; Zhang, S.; Duan, P.; Liu, Q.; Niu, S.; Dong, D.; Hu, X. Impacts of externally added Brønsted and Lewis acid on conversion of furfural to cyclopentanone over Ni/SiC catalyst. *Mol. Catal.* **2020**, *496*, No. 111187.
(31) Shen, D.; Zhao, J.; Xiao, R. Catalytic transformation of lignin to aromatic hydrocarbons over solid-acid catalyst: Effect of lignin sources and catalyst species. *Energy Convers. Manage.* **2016**, *124*, 61−72.
(32) Wang, Y.; Tang, Z.; Chen, M.; Zhang, J.; Shi, J.; Wang, C.; Yang, Z.; Wang, J. Effect of Mo content in Mo/Sepiolite catalyst on catalytic depolymerization of Kraft lignin under supercritical ethanol. *Energy Convers. Manage.* **2020**, *222*, No. 113227.
(33) Wang, Y.; Huang, Y.; Liu, L.; He, L.; Li, T.; Len, C.; Yang, W. Molecular oxygen promoted synthesis of methyl levulinate from 5-hydroxymethylfurfural. *ACS Sustainable Chem. Eng.* **2020**, *8*, 14576−14583.
(34) Zhang, Z.; Dong, K.; Zhao, Z. Efficient Conversion of Furfuryl Alcohol into Alkyl Levulinates Catalyzed by an Organic−Inorganic Hybrid Solid Acid Catalyst. *ChemSusChem* **2011**, *4*, 112−118.
(35) Bernal, H. G.; Benitob, P.; Rodríguez-Castellónc, E.; Gallettia, A. M. R.; Funaioli, T. Synthesis of isopropyl levulinate from furfural: Insights on a cascade production perspective. *Appl. Catal., A* **2019**, *575*, 111−119.
(36) Tiwari, M. S.; Gawade, A. B.; Yadav, G. D. Magnetically separable sulfated zirconia as highly active acidic catalyst for selective synthesis of ethyl levulinate from furfuryl alcohol. *Green Chem.* **2017**, *19*, 963−976.
(37) Chaffey, D. R.; Bere, T.; Davies, T. E.; Apperley, D. C.; Taylor, S. H.; Graham, A. E. Conversion of levulinic acid to levulinate ester biofuels by heterogeneous catalysts in the presence of acetals and ketals. *Appl. Catal., B* **2021**, *293*, No. 120219.
(38) Li, Z.; Zuo, M.; Jiang, Y.; Tang, X.; Zeng, X.; Sun, Y.; Lei, T.; Lin, L. Stable and efficient CuCr catalyst for the solvent-free hydrogenation of biomass derived ethyl levulinate to γ-valerolactone as potential biofuel candidate. *Fuel* **2016**, *175*, 232−239.
(39) Babaei, Z.; Chermahini, A. N.; Dinari, M. Alumina-coated mesoporous silica SBA-15 as a solid catalyst for catalytic conversion of fructose into liquid biofuel candidate ethyl levulinate. *Chem. Eng. J.* **2018**, *352*, 45−52.
(40) Karnjanakom, S.; Maneechakr, P.; Samart, C.; Guan, G. Ultrasound-assisted acetylation of glycerol for triacetin production over green catalyst: A liquid biofuel candidate. *Energy Convers. Manage.* **2018**, *173*, 262−270.
(41) Maneechakr, P.; Karnjanakom, S. Selective conversion of fructose into 5-ethoxymethylfurfural over green catalyst. *Res. Chem. Intermed.* **2019**, *45*, 743−756.
(42) Zhang, J.; Liu, Y.; Yang, S.; Wei, J.; He, L.; Peng, L.; Tang, X.; Ni, Y. Highly Selective Conversion of Furfural to Furfural Alcohol or Levulinate Ester in One Pot over ZrO2@SBA-15 and Its Kinetic Behavior. *ACS Sustainable Chem. Eng.* **2020**, *8*, 5584−5594.
(43) van der Waal, J. C.; Kunkeler, P. J.; Tan, K.; Bekkum, H. Zeolite titanium beta: A selective catalyst in the meerwein-ponndorf-verley-oppenauer reactions. *Stud. Surf. Sci. Catal.* **1997**, *110*, 1015−1024.
(44) Liu, X.; Pan, H.; Zhang, H.; Li, H.; Yang, S. Efficient Catalytic Upgradation of Bio-Based Furfuryl Alcohol to Ethyl Levulinate Using Mesoporous Acidic MIL-101(Cr). *ACS Omega* **2019**, *4*, 8390−8399.

https://doi.org/10.1021/acssuschemeng.1c04606
ACS Sustainable Chem. Eng. XXXX, XXX, XXX−XXX